Drumlin formation within the Bustarfell drumlin field, NE-Iceland: Integrating sedimentological and ground-penetrating radar data

Drumlin formation within the Bustarfell drumlin field

Nína Aradóttir[1](nia1@hi.is), Ívar Örn Benediktsson[1](ivarben@hi.is), Ólafur Ingólfsson[1](oi@hi.is), Erik Sturkell[2](erik.sturkell@gvc.gu.se), Skafti Brynjólfsson[3](skafti.brynjolfsson@ni.is), Wesley R. Farnsworth[1,4](wesleyf@hi.is), Emrys Phillips[5](erp@bgs.ac.uk)

[1]*Institute of Earth Sciences, University of Iceland, Sturlugata 7, Is-102 Reykjavík*

[2]*Department of Earth Sciences, University of Gothenburg, 405 30 Gothenburg Sweden*

[3]*Icelandic Institute of Natural History, Borgir við Norðurslóð, 600 Akureyri*

[4] *Globe Institute, University of Copenhagen, Øster Voldgade 5, DK-1350 Copenhagen Denmark*

[5]*British Geological Survey, The Lyell Centre, Research Avenue South Edinburgh, EH14 4AP, UK*

Corresponding author: nia1@hi.is (Nína Aradóttir)

Drumlins are important bedforms of former glaciated landscapes as they demonstrate past ice-flow directions and elucidate processes that operated at the ice/bed interface. Recently mapped drumlins and other streamlined subglacial bedforms in NE-Iceland reveal the flow-sets of cross-cutting palaeo-ice streams that were active within the Iceland Ice Sheet (IIS) during and following the Last Glacial Maximum. Here we study the Bustarfell drumlin field within the Vopnafjörður-Jökuldalsheiði flow-set. The internal architecture of two drumlins was investigated using sedimentological analysis and ground-penetrating radar (GPR, 50 and 100 MHz) to illuminate subglacial processes that contributed to drumlin formation, as well as the history and dynamics of the IIS. On the stoss side of one of the drumlins, two subglacial traction till units were identified, separated by a thick unit of deformed glaciofluvial sand and gravel. The core of glaciofluvial material suggests that the drumlin formed around well-drained patches (sticky spots) in the subglacial bed that retarded the ice flow locally through increased basal drag and encouraged till deposition. Furthermore, our GPR data indicate a combination of erosional and depositional processes. We suggest that the glaciofluvial sediments were deposited as small ice-marginal fans on the Bustarfell plateau, possibly during the Bølling-Allerød interstadial, and that the drumlins were formed around these fans during a subsequent readvance during the Younger Dryas.

Keywords: Drumlin; Subglacial processes; Ground-penetrating radar; Iceland Ice Sheet; Bustarfell

1. Introduction

Drumlins are subglacial bedforms that have been studied to a great extent for palaeoglaciological reconstructions and as indicators for glacier dynamics (e.g. Menzies, 1979; Stokes, 2018). They commonly occur at palaeo-ice streams beds in conjunction with other streamlined subglacial bedforms (SSBs), such as mega-scale glacial lineations (MSGLs) and mega-flutes (e.g. Clark, 1993; Hart, 1999; Stokes and Clark, 1999; 2002; Briner, 2007) but have also been observed under contemporary ice streams (Smith, 1997; King et al., 2007; Smith et al., 2007) and in recently exposed forefields of retreating glaciers (Johnson et al., 2010; Benediktsson et al., 2016; Jónsson et al., 2016; Allaart et al., 2018). Because direct observations of processes operating under contemporary ice streams are limited to borehole and seismic investigations (King et al., 2007; Stokes, 2018), the geomorphology and composition of palaeo-ice stream beds is critical for our understanding of the formation of SSBs and the dynamics and mechanism of ice streaming (Stokes and Clark, 1999, 2001; Livingstone et al., 2012; Stokes, 2018).

Drumlin composition can vary significantly between and within drumlin fields, as the drumlins can be composed of till, stratified sand and gravel, bedrock, or a combination of all (see Stokes et al., 2011). The typical shape of a drumlin is a smooth, streamlined hill (Menzies, 1979), even though recent studies have highlighted more diverse morphologies (Spagnolo et al., 2010; Maclachlan and Eyles, 2013). Drumlins exhibiting a wide range of composition and morphological characteristics have led to several hypotheses of their formation; including deformation of till around more competent cores (Smalley and Unwin, 1968; Boulton, 1987; Hart, 1997), catastrophic meltwater floods (Shaw, 2002), and instabilities at the flat bed causing a rise in the till surface (Hindmarsh, 1998; Fowler, 2000, 2010, 2018; Stokes et al., 2013; Fowler and Chapwanya, 2014). Hart (1997) classified drumlins into three types and suggested that they can be formed by either erosion, deposition, or deformation, or a combination of all, although others have explained their formation to be solely erosional (Eyles et al., 2016; Hermanowski et al., 2019). The discussion concerning their formation has evolved towards whether their formation can be explained by a unifying theory (Clark, 2010; Stokes et al., 2011) or if the variety and complexity of drumlin composition indicates that different processes can lead to a similar morphological expression (Möller and Dowling, 2016).

Studies of the internal architecture and composition of SSBs are restricted to open, accessible sections in the field. And thus geophysical instruments, such as ground-penetrating radar (GPR), have increasingly been used to integrate geophysical data with lithostratigraphic and sedimentological data (e.g. Bristow and Jol, 2003; Cassidy et al., 2003; Kjær et al., 2004; Neal, 2004; Benediktsson et al., 2009; Watts et al., 2022). For recent examples, Spagnolo et al. (2014) successfully applied GPR on drumlins in Scotland to investigate, the relationship between the internal architecture of the drumlins to their substrate and inter-drumlin areas and providing recommendation for future investigations. Woodard et al. (2020) correlated GPR profiles with stratigraphic logs to shed light on drumlin architecture and formation within the recently exposed drumlin field at Múlajökull, Iceland, which supports previous conclusion that they formed through both depositional and erosional processes.

Ice streams are considered to have been present within the Iceland Ice Sheet (IIS) during and following the Last Glacial Maximum (LGM). Their existence has to a large extent been based on modelling (Bourgeois et al., 2000; Hubbard et al., 2006; Patton et al., 2017), which has been further supported with onshore and offshore geomorphological mapping of SSBs, glacial striae and large-scale topography (Spagnolo and Clark, 2009; Clark and Spagnolo, 2016; Principato et al., 2016; Norðdahl et al., 2019; Benediktsson et al., 2021b, 2022a; Fig. 1A). Principato et al. (2016) mapped and quantified the properties of SSBs in NW-Iceland, significantly improving the understanding of the dynamics and extent of palaeo-ice streams in this region. A recent study by Benediktsson et al. (2022a) on SSBs in NE-Iceland revealed a pattern of cross-cutting palaeo-ice streams that reflect shifts in ice sheet dynamics and the migration of ice divides. Despite this recent effort in investigating drumlins and other SSBs in Iceland, no previous studies have focused on the internal architecture of drumlins formed during the last glaciation/deglaciation.

The aim of this paper is to investigate the internal architecture and composition of drumlins within the Bustarfell drumlin field by integrating sedimentological analysis and GPR profiling. Furthermore, we address the processes leading to regional drumlin formation as well as enhance our understanding of the glacial history and dynamics of the IIS in NE-Iceland.

2. Setting

The Bustarfell drumlin field is located on a plateau at 400-550 m a.s.l. between the Hofsárdalur and Vesturárdalur valleys within the Vopnafjörður valley-fjord system in NE-Iceland. The regional bedrock consists primarily of Miocene and Pliocene (>3.3-0.8 million years old) basalt lavas with intercalated sediments, with ages that become progressively younger towards the west. The basalt bedrock strikes gently towards the north (Sæmundsson, 1977, Jóhannesson and Sæmundsson, 2009). The Vopnafjörður fjord and valleys have been carved into the bedrock during frequent glaciations during the Quaternary period (Sæmundsson, 1995; Benediktsson et al., 2021a). The valleys are orientated SW-NE and are over 30 km long from the coast towards the highlands. The Bustarfell plateau is relatively flat with numerous peat bogs, except for three bedrock hills (Bustarfell, Urðarfell and Kálfafell) (Figs 1B & 2A). Large angular to subangular boulders, up to 4 m in diameter, are common in the drumlin field, especially in the SE part of the area. Drift thickness in the area has not been mapped but frequent bedrock outcrops suggest discontinuous sediment cover and that the drift is generally thin between the drumlins. The bedrock is frequently glacially scoured and striated, with orientation towards the NE.

Palaeo-ice stream flow-sets in NE-Iceland were reconstructed based on the mapping of nearly 1000 SSBs (drumlins and MSGLs) that define cross-cutting palaeo-ice streams that operated during and following the LGM. The drumlins from the Vopnafjörður-Jökuldalsheiði flow-set (310 mapped bedforms) exhibit a large-scale converging pattern with variable directions in the highlands that align towards northeast in the central part, parallel to the Vopnafjörður valleys and fjord (Fig. 1B). The Bustarfell drumlin field is situated in the center of the Vopnafjörður-Jökuldalsheiði palaeo-ice stream flow-set (Benediktsson et al. 2022a).

Limited chronological data exist on the extent of the IIS in NE-Iceland but based on thermomechanical modelling experiments by Patton et al. (2017), the IIS reached its maximum extent at the shelf edge around 22.9 ka BP and a rapid marine deglaciation initiated at around 21.8 ka BP. The abrupt warming at the Bølling Interstadial (14.7-14.1 cal. ka BP) during the deglaciation resulted in a collapse of the ice sheet offshore (Ingólfsson and Norðdahl, 2001; Norðdahl and Ingólfsson, 2015). Subsequently, two readvances occurred, during the Younger Dryas period (YD) (12.9-11.7 cal. ka BP) and Early Preboreal (10.3-9.0 cal. ka BP). Previous studies in NE-Iceland have mainly focused on the deglaciation and shoreline displacement after the YD (Norðdahl and Hjort, 1993; Sæmundsson, 1995). The ice-margin has been suggested to have been situated at the mouth of the Vopnafjörður valley during the YD, but ice-marginal deltas indicate small readvances or stillstands of the ice margin farther up-valley in Vesturárdalur and Hofsárdalur during the Preboreal (Fig. 1B; Sæmundsson, 1995).

3. Methods

3.1 Geomorphological mapping and morphological analysis

The geomorphological mapping (Figs 1B & 2A-C) of the drumlins at Bustarfell was initially performed by Benediktsson et al. (2022a) but reviewed and refined for this study. The mapping was based on the Arctic Digital Elevation Model (ArcticDEM) with a 2 m vertical and <1 m horizontal resolution (PGC, 2018; corrected and mosaicked by the National Land Survey of Iceland (NLSI), the Icelandic Met Office, and the Polar Geospatial Center (PGS)). Furthermore, mapping was aided by infrared Spot satellite images with 2.5 m resolution from NLSI and aerial images from Loftmyndir ehf. Analysis of the data and mapping was conducted in ESRI ArcGIS 10.4-7 and finalized in Canvas X. In addition, channels incising through the drumlins were mapped for this study, using the criteria from Greenwood et al. (2007). To investigate the morphology of the drumlins, the length of the long axis, the width orthogonal to the long axis, and the orientation of the long axis were measured for each bedform using the minimum bounding geometry tool in ArcGIS, as described by Napieralski and Nalepa (2010).

3.2 Sedimentology

Natural sections through drumlins in the area are rare and only one natural coastal section could be cleaned by hand and studied (T4); on the flank of drumlin Thury. An excavator was used to dig three pits (T1-3) in drumlin Thury, all located in dry transverse channels (Fig. 2B). Sediments exposed in the sections were documented at a scale of 1:20, using the data chart by Krüger and Kjær (1999) for glacial sediments, and the strike and dip of beds/structures were measured. Clast fabric measurements were collected from a 25x25 cm surface at each site, where the dip and dip direction were measured for at least 25 elongated clasts (a:b ratio >1.5:1) with an a-axis ranging in length from 0.6 to 6 cm (Kjær and Krüger, 1998). The measurements were then plotted and analyzed in the software Stereonet and the eigenvectors (S_1 and S_3) and eigenvalues (V_1) calculated. If the eigenvalue of the principal eigenvector was higher than 0.54, the clasts were considered to show preferred orientation (Lawson, 1979). All compass measurements were corrected for the regional negative declination of 10°C (in 2020). The sections and additional data were illustrated in Canvas X.

Grain-size analyses of diamict units were carried out using standard sieving methods, starting by washing out materials finer than 0.063 mm (fines; clay and silt), followed by dry sieving to separate sand and gravel fractions. To examine the clast morphology, fifty clasts, with an a-axis between 1.5 to 10 cm, were collected from 25x25 cm surfaces. The a (long)-, b (intermediate)- and c (short)-axes were measured and plotted in a ternary diagram (Evans and Benn, 2004). In addition, the roundness and texture of the clast was estimated (Powers, 1953; Evans and Benn, 2004). The clast shape is presented as the C_{40} index (percentage of clasts with c:a axis ratio ≤ 0.4) and the clast roundness as the RA index (percentage of angular and very angular clasts) (Benn and Ballantyne, 1993).

3.3 Ground-penetrating radar

GPR profiles were acquired on two drumlins, Thury and Foss (Figs 2B-C), with a Malå Ramac/GPR CUII using both 50 and 100 MHz antennas, and antenna separation of 4 and 0.6 m, respectively. Surveys were made with a step size ranging from 0.02 to 0.5 m (Table 1). The data collection window was 0-715 ns for 50 MHz and 0-218 ns for 100 MHz and the sampling frequency was approximately 10 times the antenna frequency. In total, twenty profiles were acquired with a total length of 6437 m, transverse, longitudinal and diagonal, across the targets (Table 1). Part of the profiles from drumlin Thury were collected along the sections (Fig. 2B) in order to facilitate correlation between the GPR profiles and the sections. Data were processed with

ReflexW 8.0 Sandmeier software, a GPR and seismic processing software, and topographic data from the ArcticDEM were used to rectify the profile elevation. The processing steps were done in this order (when deemed beneficial): dewowing, move start time, energy decay, background removal and elevation correction (see supplementary data). A velocity of 0.084 m/ns was used for depth conversion of the recorded two-way travel time based on common mid-point (CMP) measurements on drumlin Sauralda in Bakkaflói (Fig. 1B). This value is similar to other glacial sediments in Iceland (Cassidy et al., 2003; Kjær et al., 2004; Benediktsson et al., 2009; Woodard et al., 2020) and to the tabulated range of 0.06-0.1 m/ns for saturated and damp sand (Jol and Bristow, 2003).

4. Results

4.1 Morphology of the drumlins

In total, 77 drumlins occur within the Bustarfell drumlin field, an area of ~100 km^2. The mean orientation of the drumlins is SW-NE (36°), The mean length is 696 m with a range of 319-1438 m and the mean width is 183 m with a range of 86-301 m. The mean elongation ratio (ER) is 3.8:1 with a range of 1.8:1-6.5:1 (Table 2). The histograms all demonstrate a unimodal distribution, similar to the entire data set of SSBs in NE-Iceland (Benediktsson et al., 2022a). However, the histograms for the Bustarfell drumlins do not have as clear positive skews and indicate rather consistent morphometry, with little to no difference between the mean and median values (Figs 2F; Table 2). Compared to the mapped drumlins in NE-Iceland, the Bustarfell drumlin field is well-defined with a relatively high density of 7-9 drumlins per 4 km^2 (Benediktsson et al., 2022a). Peat bogs are common in the inter-drumlin areas and, occasionally, link with seasonal drainage channels. Often these drainage channels correspond to transverse depressions cutting perpendicular through the drumlins (Figs 2A, D, E). Given the morphology and re-occurring interval of the transverse channels (Figs 2A, D, E), we associate these features with ice-marginal positions and meltwater incision during stepwise glacial retreat and drumlin exposure from under the ice (cf. Greenwood et al., 2007).

Two drumlins within the Bustarfell drumlin field were investigated in detail: drumlin Thury and drumlin Foss. Drumlin Thury is in the northeastern part of the drumlin field and is orientated SW-NE (46°). The drumlin is around 600 m long, 160 m wide and up to 12 m high with an ER of 3.6:1. The longitudinal profile of the drumlin is asymmetric with a reversed shape (lee side higher than the stoss side) and has been subdivided by two large, transverse meltwater channels, each over 50 m in width and around 3-4 m deep with ~180 m spacing between them (Figs 2A, B). Drumlin Foss is located within the western part of the drumlin field, northeast of Kálfafell, and is orientated SSW to NNE (32°). It is around 840 m long, 175 m wide and up to 8 m high with an ER of 4.8:1. The longitudinal profile of the drumlin is nearly symmetric. Five transverse, shallow (< 2 m deep) meltwater channels can be identified in the surface of drumlin Foss with incision either half-way or completely through the drumlin. The spacing between the channels varies from 70-180 m (Figs 2A, C).

4.2 Sedimentology

Four sections were logged in drumlin Thury (T1-T4; Figs 2B, 3, 4) with six lithofacies identified: (f1) clayey-gravelly, grey diamict; (f2) silty-sandy, dark/blue-grey diamict; (f3) sand and gravel; (f4) silt, sand and gravel; (f5) soil; (f6) gravelly, brownish diamict. Lithofacies codes are according to Krüger and Kjær (1999) (Fig. 3).

4.2.1 F1, clayey-gravelly, grey diamict [Dm/h/b/M/F($m_{1\text{-}3}$)2-4] - The main deposit in sections T1-3 in drumlin Thury is a grey, firm, moderate to clast-rich diamict with clayey to gravelly matrix. It is generally homogenous, but areas of banded and heterogeneous matrix appear. The clast content generally decreases in the lower part of the sections and the matrix becomes firmer. Examination of clasts in the field and the clast morphology show that they are to a large extent blocky and subrounded to subangular (C_{40} = 0-16 and RA = 0-2). Occasional bullet-shaped and striated clasts occur (18-26%). Based on three grain size analysis from two sections (T2 and T3) the matrix ranges from; 32-54% fines, 30-35% sand, 16-35% gravel. The grain-size analysis of f1 does not show any significant change between the sections, although section T2 has greater content of fines than the other sections and T3 slightly more gravel. Poorly developed fissility was observed sporadically. Lenses and bands of stratified sand and gravel (f4), often showing sign of deformation, commonly occur within the lithofacies (Figs 3B, 4B & 6A-D). F1 is interpreted as subglacial traction till deposited by a combination of deformation and lodgment, based on its characteristics, fissility, clast morphology, fabric, and deformed inclusions (Krüger and Kjær, 1999; Evans et al., 2006).

4.2.2 F2, silty-sandy, dark/blue-grey diamict [DmM(m_2)3] – This lithofacies is a massive, homogenous, matrix-supported diamict with a silty-sandy matrix and a moderate clast content, and is only observed in section T4 (Figs 4B & 5). It is firm and rather difficult to excavate. The colour of the lithofacies is dark/blue-grey, which differentiates it from f1. Based on the grain size distribution it contains 31% fines, 46% sand and 22% gravel and the clasts are usually blocky and subrounded to subangular (C_{40} = 5 and RA = 2) and below 15 cm in diameter. Larger boulders (<30 cm in diameter) also do occur. No structures were observed in the diamict but a few lenses of laminated/rippled sand (f4) occur within it (Figs 4B & 6F). Based on its characteristics and presence of sand lenses within it, f2 is interpreted as subglacial traction till (Krüger and Kjær, 1999; Evans et al., 2006).

4.2.3 F3, sand and gravel [S/G/m/h/p] – This lithofacies represents layers (~5-100 cm thick) of sorted sand and gravel that are observed in sections T1 and T4 (Figs 6C-D & 5). It appears as either massive, horizontally laminated, or cross-bedded with visible deformation structures. The clasts in the gravel layers are mostly subrounded (<3 cm in diameter). We interpret f3 as glaciofluvial outwash deposits (Evans et al., 2006).

4.2.4 F4, silt, sand and gravel [*F/S/G/m/h/p]* – This lithofacies describes lenses or thin layers (<3 cm thick) of silt, sand and gravel that were observed in all of the sections within f1 and f2. F4 appears as massive or horizontally laminated, with occasional vague ripples and deformation structures (Figs 6A, D). The sand lenses are very compact, and most of the lenses are dipping towards NE, parallel to the drumlin´s long axes. The gravel is mostly subrounded, although subangular clasts are also present. F4 is interpreted to represent the infilling of smaller subglacial meltwater streams or ponds (Evans et al., 2006).

4.2.5 F5, soil [Fm] – In the upper part of sections T1-3 in drumlin Thury is a 25-200 cm thick unit of fine-grained brownish soil. Lenses of sand and gravel can be found within this lithofacies as well as dark and light-coloured, fine-grained tephra layers (Figs 6A, C). The tephra layers are usually 1-5 cm thick except for a layer in the upper part of T1 that is around 10 cm thick. The tephra was transported as air fall from various Icelandic volcanoes and deposited on the Bustarfell plateau. Although we do not have any constraint on the origin or age of the tephra layers, the ash distribution maps of the area indicate that the light-coloured layers might be Hekla 3 (3000 cal. yr BP) and 4 (4200 cal. yr BP) (Guðmundsdóttir et al., 2011). The dark layers are most likely of unknown origin from the Late Holocene.

4.2.6 F6, brownish, gravelly diamict [DmM($m_{2\text{-}3}$)1] – Brownish, massive diamict with silty to gravelly matrix is observed at the top of sections T2 and T3 and right below the soil (f5) in T2

(Figs 6A & C). It can be distinguished from f1 by the brownish colour and higher content of gravel and no boulders (>3 cm in diameter). No structures can be found within the lithofacies. F6 is interpreted as cryoturbated diamict because of its location above and below the soil (f5), structureless characteristics and the difference of clast content from f2.

4.3 Stratigraphy

4.3.1 Section T1 is located in a dry transverse ice-marginal channel at the down-ice side of drumlin Thury, close to the longitudinal axis of the drumlin (Figs 2B, D). The section is orientated SE-NW, and is 4.6 m high with four lithofacies observed. Groundwater was present at the base of the section (Fig. 6C). The lowermost part of the section (3.0-4.6 m) is composed of grey massive, till with clayey to sandy matrix (f1) with lenses of sand (f4). Very delicate fissile structures were observed in the matrix. At ~3 m depth, the till is dissected by interbedded, stratified sand to coarse gravel (<5 cm in diameter) (f3). The layer is 0.5-0.2 m thick, thickening towards the NNE and coarsening downwards. F1 appears again overlying the gravel with a sharp boundary (2.0-2.8 m). The upper till has coarser matrix (sandy to gravelly) and higher clast content than the till below and is less compact. Clast fabric in the upper part of the till (sampled at 2.5 m depth) shows preferred orientation roughly parallel to the orientation of the bedform (SW-NE), dipping towards SW (up-ice) (V_1 = 215°/42°, S_1 = 0.76) (Fig. 3B). There is a sharp conformable contact up to the uppermost 2 m of the section that are composed of brown soil (f5) with 5 light and dark tephra layers. A few outsized clasts (<1cm in diameter) occur in the lowermost part of the soil (Figs 3B & 6C).

4.3.2 Section T2 is ~40 m SSW of section T1 in the same transverse channel, southeast of the long axis and is orientated NNW-SSE (Figs 2B, D). The section is 4.6 m high with four lithofacies identified. The section is mostly composed of subglacial traction till (1.1-4.6 m: f1), with silt, sand,

and gravel lenses (f4). Fissile and small-scale ductile deformation structures appear throughout the section, with apparent dip towards NE. Clast fabrics in the upper part of the till (sampled at 1.3 and 1.6 m depth) show preferred orientation parallel and oblique to the bedform long axis, SW-NE, where clasts are dipping down-ice (V_1 = 48°/1° and 68°/6°, S_1 = 0.69 and 0.72). Above the till is a gradual boundary to f6, where there is about 0.2-0.3 m thick transition zone between clean soil and diamict. There is an abrupt change in colour between f6 and the underlying till (f1) from brown to grey. Cryoturbated diamict (f6) is at the top of the section (0-0.2 m), with gradational boundary to f5, a 0.6 m thick soil with four thin (<1 cm), cryoturbated tephra layers (Figs 3B & 6A).

4.3.3 Section T3 is located ~90 m SW of section T1, in the transverse channel that cuts through the middle of the drumlin (Fig. 2B). The section is orientated SE-NW and WSW-ENE. In total, four lithofacies were identified in the 2 m high section. Most of the section (0.6-2 m) is composed of massive, silty-sandy till (f1), that becomes less compact in the uppermost part of the section. Vague fissility and laminated sand lenses (f4) are identified in the upper part of the section (Fig. 6B). Two clast fabrics were done in this section. One of them (sampled at 0.8 depth) shows preferred orientation parallel to the bedform, SW-NE, with clasts dipping towards SW/SSW (up-ice) (V_1 = 223°/17°, S_1 = 0.82), whereas the other one (sampled at 0.9 m depth) showed preferred orientation oblique to the long axis of the bedform (V_1 = 196°/18°, S_1 = 0.79). The upper part of the section is composed of brownish soil (0.25-0.6 m: f5) with few tephra layers and cryoturbated diamict (0-0.25 m: f6) is at the top The contact between all the lithofacies is sharp (Fig. 3B).

4.3.4 Section T4 is located by the lake at the stoss side of drumlin Thury and is orientated W-E, i.e. obliquely to the drumlin long axis. In total, the section is around 40 m long and was documented in five stratigraphical logs and one diagram, in which four lithofacies were identified (Figs 2B, 4A, B & 5; T4.1-6). T4.1 is located at the western end of the section at the break of slope of the drumlin and is only 0.8 m high. It consists of silty-sandy, massive, dark-grey till (f2) with small lenses of sand (f4) (Fig. 6F). Two fabric analysis (sampled at 0.3 and 0.5 m depth) show preferred orientation towards the north (V_1 = 7°/16° and 354°/30°, S_1 = 0.71 and 0.76) (Fig. 4B). T4.2 is located ~25 m east of T4.1 and is illustrated on Fig. 5. The section is up to 2 m high and massive, compact, blue-grey till (f2) is observed partly at the base (<0.25 m thick). Most of the section above is composed of blue-grey to brown, massive sand to gravel (f3), with deformed layers and lenses of laminated gravel, sand and silt (f4). Small-scale normal faults and an upright fold were also observed, indicative of both brittle and ductile deformation (Figs 5 & 6E). Smaller cobbles (5-15 cm in diameter) and larger boulders (>30 cm in diameter) are embedded in the till. Slightly further to the east are sections T4.3 and T4.4, that show similar stratigraphy as T4.2, although T4.4 does have over 1 m of subglacial traction till (f1) at the top with a sharp boundary to the sand and gravel below (f3). Sections T4.5-6 are ~8-10 m farther to the east with similar stratigraphy as the sections to the west. Interbedded, laminated, rippled, cross-bedded to massive sand and gravel beds, showing signs of deformation (f3), make up the lowermost part of the sections (1.2-2 m thick). Large boulders (>20 cm in diameter) are lodged into the sorted sediments. The boundary is sharp with the overlying subglacial traction till (f1;1-1.9 m thick). Occasional sand lenses (f4) are found within the subglacial traction till (Figs 4B, D & 6D).

4.4 Ground-penetrating radar

Twenty GPR profiles were collected with 50 and 100 MHz antennas (Figs 2B, C, Table 1). Here, we show six transverse profiles that are considered to be representative of the drumlin architecture and the remaining profiles. The different radar facies and structures that are identified within the profiles are described and labelled in Table 3.

4.4.1 Drumlin internal architecture

On the 50 MHz profiles, the interior of the drumlins can be described in general as wavy with moderately continuous to discontinuous reflections (radar facies B.1) that can be traced down to a maximum depth of ~16 m. On the 100 MHz profiles, one radar facies (B.2) could also be identified; chaotic, moderately continuous to discontinuous reflections (Table 3; Figs 3C, 4C & 7). Although the reflection pattern between the two frequencies varies slightly as they have different resolution, we interpret the radar facies in a similar manner, based on their characteristics and correlation with the stratigraphical logs (Figs 3B, C & 4B, C). Radar facies B.1 and B.2 are interpreted as subglacial traction till with interbedded glaciofluvial material of various thickness. Different structures are identified within the radar facies, such as concave and convex structures and occasional hyperbolas (Table 3; Figs 3C, 4C & 7A, C). The hyperbolas (B.3) are interpreted as larger boulders or boulder clusters in the till and the concave and convex structures as channel infillings (C.1 and C.2) (Neal, 2004). The chaotic structure might represent the deformation of the sediments that was observed in the sections (Neal, 2004; Watts et al., 2022), and explain why it is challenging to distinguish between the till and the glaciofluvial material. The direct air- and ground-waves in the 50 MHz profiles appear as strong arrivals at the top, followed by another strong arrival that we interpret to be the groundwater table, as it correlates with the depth of the groundwater table (at 4-5 m) observed in section T1 (Fig. 6C). These strong arrivals hamper a straight-forward correlation with the excavated sections.

Three general patterns can be detected from the transverse profiles; 1) Profiles from both drumlins show outward-dipping, long reflections that are conformable with the surface of the drumlins (Figs 3C & 7). 2) On one or both flanks of drumlins Thury and Foss, the outward-dipping reflections cut either shallower-dipping or inward-dipping, shorter reflections below. This is visible from both the lee side on drumlin Thury (Fig. 3C) and the stoss side on drumlin Foss (Fig.

7C). However, due to the interference of the air- and ground wave and the groundwater table in the upper part of the profiles (3-4 m), the extent of patterns no. 1 and 2 are not entirely understood. 3) The general appearance of the reflections are slightly stronger and less chaotic on the stoss side and at the base of the profiles (Figs 3C & 7). Other studies have interpreted stronger and more prominent reflections as higher concentration of sorted material (e.g. Stokes et al., 2008; Woodard et al., 2020).

4.4.2 Boundary to the substratum

In a part of the 50 MHz profiles from drumlin Foss, strong reflections (radar structure A) are identified below radar facies B.1. The radar structure is planar to wavy and moderately continuous. In drumlin Foss the reflection generally occurs at 10-12 m depth, with little to no difference between the stoss and the lee side but is curved up towards the ESE on the transverse profiles. No coherent radar returns are beneath radar structure A (Figs 7A, C; Table 3). This structure is interpreted to be the surface of the bedrock in the area, similar to other studies on drumlin's internal architecture with GPR (Spagnolo et al., 2014). Based on its (strong reflective) characteristics and wavy structure, it is suggested that the bedrock has been sculptured by ice. No bedrock outcrops are seen in close vicinity of the investigated drumlins; however, the general appearance of bedrock exposures in the area is supportive of our interpretation. There are several potential reasons why the strong reflection is not seen in drumlin Thury, such as the thickness or the characteristics of the sediment (e.g., higher clay content) preventing deeper penetration, or lower data resolution (Jol and Bristow, 2003; Spagnolo et al., 2014).

4.4.3 Inter-drumlin areas

Most of the GPR profiles extend beyond the break of slope of the drumlins (Figs 2B, C) and indicate that the drumlin form extends below on-lapping sediments in the inter-drumlin areas.

These areas are characterized by radar facies D, which comprises numerous parallel (vague) reflections that range from being continuous to discontinuous (Table 3; Figs 3C & 7A, C). This facies is interpreted to be post-glacial sediments with thickness up to 8 m. Based on field observation, the uppermost part of the facies can be classified as peat bog (Figs 2D, E). The peat bog extenuates the original morphology of the drumlins, especially their height (Spagnolo et al., 2012; 2014; Finlayson, 2013; Benediktsson et al., 2016).

4.5 Correlation between sections and GPR profiles

Although the GPR profiles were surveyed in the vicinity of the sections, precise correlation between them was challenging, most likely due to sediment deformation and the lack of radar structures or facies that could be used as markers. The ground- and air-waves and the groundwater table interfere with the upper 3-4 m of the profiles, thus affecting the precise correlation of the GPR data to the stratigraphical logs. However, without the sections in drumlin Thury, the interpretation of the GPR profiles would have been more demanding as the radar facies interpretation is to a great extent based on the sections. We do therefore assume that the sections are representative for the drumlin composition at greater depth, as no clear boundaries or different units could be identified on the GPR profiles. Certain structures correlated well between the 50 and 100 MHz antennas from drumlin Foss as illustrated in Figure 7.

5. Discussion

5.1 Internal architecture

The investigated drumlins on Bustarfell can be classified as part till/part sorted sediment drumlins (type 4 in Stokes et al., 2011). Although the boundary to the underlying bedrock could probably be detected with the GPR on drumlin Foss, the drumlins do not comprise an actual bedrock core but rather seem to rest on the bedrock surface. The sections at the lee side and in the middle of drumlin Thury (sections T1-3) are composed of subglacial traction till, interbedded with lenses or layers of glaciofluvial material, showing signs of deformation. At the stoss side (section T4), thick, deformed glaciofluvial material appears between two tills. Our GPR profiles show slightly more prominent reflections at the stoss side, which supports that the glaciofluvial material is more abundant at the stoss side than the lee side (e.g. Stokes et al., 2008; Woodard et al., 2020). The deformation in drumlin Thury is generally more intense and extensive at the stoss side with most deformation structures classified as ductile and compressional, except for a few small normal faults indicating minor extensional deformation. The general orientation of the deformation structures indicates stress from the SW. Although individual deformational structures could not be identified on the GPR profiles, the generally chaotic pattern is considered to be representative of intensive deformation (Neal, 2004). Based on the sedimentological data alone, there is no evidence for unconformities between the subglacial traction till and glaciofluvial material. Nor does the data reveal multiple till units that would suggest depositional processes during the drumlin formation (Benediktsson et al., 2016). GPR data from other drumlin fields (Spagnolo et al., 2014; Woodard et al., 2020) have demonstrated erosional unconformities at the stoss side and flanks, and down-ice dipping reflections on the lee side indicating deposition. Our data do not exhibit the same clear evidence of depositional or erosional processes; however, minor unconformities seem to occur on one or both flanks of drumlin Thury and Foss where shorter internal reflections are truncated by the outward-dipping reflections conforming to the drumlin shape (Figs 3C & 7C). This suggests that both erosional and depositional processes are involved in the drumlin formation (Woodard et al., 2020). According to Iverson et al. (2017), such cross-cutting relationships within drumlins reflect till deposition during active flow, and erosion by regelation infiltration or meltwater in subglacial channels during quiescence or slow flow. The architecture and cross-cutting relationships in the two investigated drumlins on Bustarfell may, therefore, indicate separate phases of erosion and deposition related to glacier flow dynamics.

The clast fabrics in lithofacies 1 in section T1-3 in drumlin Thury all show unimodal and clustered fabric shapes with preferred orientation (S_1 = 0.69-0.82). Three out of the five clast fabric measurements are roughly parallel to the drumlin long axis, dipping either up-ice or down-ice, and the other two are oblique to the orientation of the drumlin. A systemic pattern of preferred orientation cannot be detected from the number or location of the clast fabrics in the section T1-3 (Fig. 3). However, the clast fabrics in lithofacies 2 in section T4.1, is orientated towards the north (353° and 7°) rather than northeast. Benediktsson et al. (2022a) suggested that the regional ice flow during a phase of maximum glaciation was towards the north independent of underlying topography. Thus, it may be speculated if the northward orientated clast fabrics in the lowermost till may result from this phase. This could be further supported by the location of the till unit in T4.1 at the edge of the drumlin's stoss side, which may suggest that it was not influenced during the drumlin-forming process, and that its sedimentological characteristics are different from the overlying till units which certainly constituent parts of the drumlin.

5.2 Formation of the drumlins and conceptual model

Sticky spots on the beds of glaciers are well-drained patches where the resistance to basal sliding is higher than in well-lubricated, low-strength areas around them, generating strain gradients across the bed (e.g. Boulton, 1987; Alley, 1993; Piotrowski et al., 2004; Stokes et al., 2007). Boulton (1987) attributes drumlins to strain gradients that lead to accretion on their top and downstream end but erosion along their periphery. The sticky spot model has thus been used to explain the formation of drumlins, e.g. under non-surging and surging glaciers in southeast Iceland (Boulton, 1987; Evans and Twigg, 2002; Waller et al., 2008; Jónsson et al., 2016) as well as on palaeo-ice stream beds elsewhere (e.g. Menzies and Brand, 2007; Evans et al., 2015; Menzies et al. 2016). The glaciofluvial material in the core of drumlin Thury suggests a pre-existing obstacle in the substratum that acted as a sticky spot and facilitated the formation of the drumlin. The unimodal shape of the Bustarfell drumlins, their high density and similar morphometry (Figs 2A-F; Table 2) does suggest to us that they were all formed by alike processes. However, we acknowledge that our data are spatially limited within the Bustarfell drumlin field and stress that this inference could be tested with more extensive excavations and GPR profiling across the field.

Dowling (2016) demonstrated that pre-existing obstacles, which could serve as drumlin cores, are necessary for the initiation of drumlin formation in areas characterized by thin glacial drift and where bedrock knobs are lacking. If obstacles, like glaciofluvial outwash exist, then drumlin formation is initiated through differential flow over and around them (Boulton, 1987). Further growth and shaping are then dependent on the physical characteristics of the substratum, till accretion and rheology, hydrology, and ice, and the subsequent architecture of the drumlin is the result of the interplay between deposition, erosion, and deformation (Hart, 1997; Möller and Dowling, 2016). Recent investigation of a modern drumlin field at Múlajökull, central Iceland, suggests that lower effective stresses occur on drumlins than between them, resulting in till accretion on their top and lee slope during surge events but erosion on drumlin heads and flanks during quiescent flow (Benediktsson et al., 2016; McCracken et al., 2016; Iverson et al., 2017). These drumlins are thus mostly composed of multiple till units with erosional unconformities. This model may be partly applicable to the drumlins at Bustarfell, but it cannot explain the initiation of their formation, which we consider to be related to pre-existing glaciofluvial material.

Based on our observations of two drumlins within the Bustarfell drumlin field, we propose the following conceptual model for their formation (Fig. 8):

A) During a maximum glaciation, subglacial traction till was deposited on Bustarfell, possibly during a phase of northward flow across the site, as discussed by Benediktsson et al. (2022a) and indicated by the clast fabrics in the lowermost till unit at drumlin Thury.

B) The ice sheet margin retreated onshore and inland during the deglaciation with meltwater being released from the glacier margin. We surmise that the glaciofluvial sediment observed within drumlin Thury was deposited proglacially during episodic retreat of the ice margin. Possibly, a sandur formed across the entire plateau with extensive braid bars that later acted as sticky spots during drumlin formation. However, due to the regional topography, we assume that the main volume of the meltwater went down the valleys on each side of Bustarfell and less water was released up on the plateau. Hence, we consider it more likely that the glaciofluvial material represents minor outwash fans deposited in front of small meltwater outlets in the retreating ice margin.

C) During a glacial readvance, the small outwash fans obstructed glacier flow and acted as sticky spots for the initiation of drumlin formation. That together with the heterogeneous surface caused velocity and strain gradients around the sticky spots, resulting in the deposition and deformation of subglacial traction till around the core.

D) Till was deposited down-glacier from the core due to low pressure shadow while erosion was effective at the periphery of the drumlin (Boulton, 1987; Hart, 1997). During the drumlin formation process, the glaciofluvial core was deformed together with the till. The deformation within both the upper till and the glaciofluvial core suggests that the drumlins were formed by subglacial deformation around a relatively weak core (Hart, 1995). The approximate alignment of the clast fabrics and deformation structures with the drumlin orientation and the conformation of the upper till with the drumlin shape suggests that the upper till accreted during rather than prior to the drumlin formation. The deformation and lenses of glaciofluvial material in the subglacial traction till, especially at the lee side of the drumlin, possibly indicates fluctuating water pressures and phases of coupling and decoupling at the ice/bed interface (Boulton et al., 2001; Kjær et al., 2006).

E) The drumlins were exposed during the final deglaciation and transverse ice-marginal channels incised the drumlin surface during a stepwise retreat of a passive terminus (Greenwood et al., 2007).

F) Post-glacial sediments have been and are deposited in the inter-drumlin areas, reducing the apparent drumlin relief (Spagnolo et al. 2012; Finlayson, 2013; Benediktsson et al., 2016).

5.3 Glacial history

Based on the present understanding of the glacial history of the Vopnafjörður area together with the conceptual model for the drumlin formation, the timing of the formation is speculated. During the LGM, the ice sheet extended all the way to the shelf edge (Spagnolo and Clark, 2009; Patton et al., 2017; Benediktsson et al., 2021b), with an ice-stream draining northwards independent of topography from an E-W orientated ice divide over the present Vatnajökull ice cap (Benediktsson et al., 2022a; Fig. 1A). The northward fabric measured in the lowermost till at the stoss side of drumlin Thury of drumlin Thury could possibly be a result of the earlier northward ice flow. Ice-sheet thinning during the following deglaciation caused a shift in the ice-sheet dynamics so that the ice flow became controlled by the topography with an ice stream flowing along the Vopnafjörður valley-fjord system towards the northeast (Benediktsson et al., 2022a). During the Bølling-Allerød interstadial, the ice sheet retreated onshore and inland to an unknown position in the eastern highlands of Iceland (Norðdahl and Pétursson, 2005; Hubbard et al., 2006; Norðdahl et al., 2008; 2012; Patton et al., 2017; Benediktsson et al., 2022b). Our data supports that

Bustarfell became ice free at that time, signified by the glaciofluvial material that we consider to have been deposited subaerially on top of the lower till. There is evidence for a glacier readvances during the YD period from numerous sites around Iceland (Norðdahl et al., 2008; Norðdahl et al., 2019; Benediktsson et al., 2022c) and Sæmundsson (1995) suggested that the readvance during the YD extended to the mouth of the Vopnafjörður valley (~17 km northeast of Bustarfell). In correlation with our conceptual model (Fig. 8), we consider the ice-contact glaciofluvial material deposition during the deglaciation to be crucial for the initiation of the drumlin formation. Consequently, we suggest that the drumlins were formed during the YD when the ice sheet readvanced and streamed across the glaciofluvial outwash. The ice-marginal channels incising the drumlins represent the final glacier retreat on Bustarfell. By assuming that they formed annually and considering their distribution and spacing, we roughly estimate that the ice margin retreated between 70-180 m/yr over the drumlin field. During the Preboreal, glaciers readvanced into the Vopnafjörður valleys resulting in the formation of ice-marginal deltas and dead-ice fields (Sæmundsson, 1995; Fig. 1B). During this less extensive phase of glacier expansion, ice did not cover Bustarfell nor affect the drumlin, protected by the (~300 m) prominence of the plateau from the valley floor.

6. Conclusion

- The investigated drumlin Thury within the Bustarfell drumlin field is composed of two units of subglacial traction till, with interbedded glaciofluvial sediments. The volume of glaciofluvial material is greater at the stoss side than the lee side, suggesting a core of glaciofluvial outwash. The upper till and the glaciofluvial sediments are clearly deformed.
- The boundary to the underlying bedrock was implied at ~10-12 m depth, based on the GPR data. There is no evidence of a bedrock core in the drumlins.

- The inter-drumlin areas are composed of postglacial sediments, up to 8 m thick. This sediment infill extenuates the original morphology of the drumlins, especially its height.
- The formation of the investigated drumlins is best explained by the sticky spot hypothesis where glaciofluvial outwash near the stoss side (essentially the drumlin core) retarded basal sliding and promoted deformation and accretion of subglacial traction till around the core and towards the drumlin tail. Our data indicate that the bedforms developed from a combination of erosional and depositional processes together with subglacial deformation.
- The unimodal shape, high spatial density, and similar morphometry of the drumlins within the Bustarfell drumlin field suggests a similar formation process.
- Correlation of the drumlin formation to the glacial history in NE-Iceland indicates that they were formed during a YD readvance. Glaciofluvial material, which accumulated on the Bustarfell plateau during deglaciation after the LGM, makes up the core of the drumlins.
- The sedimentological and GPR data are complimentary, although the deformation and lack of trace layers made the interpretation of the GPR profiles challenging. Integrating GPR data with sedimentological data in glacial environments in Iceland can be useful to investigate the internal architecture of glacial bedforms and learn about processes operating at the beds of advancing glaciers and ice sheets.

Acknowledgements. **-** This project has been funded through grants from the University of Iceland Research Fund (to ÓI), the Energy Research Fund of Landsvirkjun (to NA and ÍÖB) and the Icelandic Road and Coastal Administration (to ÍÖB). We would like to thank all our colleagues and graduate students for great company during fieldwork, constructive discussions, and helpful feedback during the project, especially for the help collecting the GPR data. Bragi Vagnsson, farmer at Bustarfell, kindly gave us the permission to excavate in drumlin Thury. The authors thank Adam Booth and an anonymous reviewer for their constructive comments that improved the manuscript.

References

Allaart, L., Friis, N., Ingólfsson, Ó., et al. 2018. Drumlins in the Nordenskiöldbreen forefield, Svalbard. Gff, 140(2), 170-188. https://doi.org/10.1080/11035897.2018.1466832

Alley R.B. 1993. In search of ice-stream sticky spots. Journal of Glaciology, 39, 447-454

Benn, D. I. & Ballantyne, C. K. 1993: The description and representation of particle shape. Earth Surface Processes and Landforms 18, 665–672.

Benediktsson, Í.Ö., Ingólfsson, Ó., Schomacker, A., et al. 2009. Formation of submarginal and proglacial end moraines: implications of ice-flow mechanism during the 1963–64 surge of Brúarjökull, Iceland. Boreas, 38(3), 440-457. https://doi.org/10.1111/j.1502-3885.2008.00077.x

Benediktsson, Í.Ö., Jónsson, S.A., Schomacker, A., et al. 2016. Progressive formation of modern drumlins at Múlajökull, Iceland: stratigraphical and morphological evidence. Boreas 45, 567-583. https://doi.org/10.1111/bor.12195

Benediktsson, Í.Ö., Brynjólfsson, S., Ásbjörnsdóttir, L. 2021a. Iceland: glacial landscapes of Iceland. In: Palacios, Hughes, García-Ruiz, Andrés: Vol. 1 European Glacial Landscapes: Maximum Extent of Glaciations. Elsevier.

Benediktsson, Í.Ö., Brynjólfsson, S., Ásbjörnsdóttir, L. 2021b. Iceland: glacial landforms from the Last Glacial Maximum. In: Palacios, Hughes, García-Ruiz, Andrés: Vol. 1 European Glacial Landscapes: Maximum Extent of Glaciations. Elsevier.

Benediktsson, Í.Ö., Aradóttir, N., Ingólfsson, Ó., et al. 2022a. Cross-cutting palaeo-ice streams in NE-Iceland reveal shifting Iceland Ice Sheet dynamics. Geomorphology, 396, 108009. https://doi.org/10.1016/j.geomorph.2021.108009

Benediktsson, Í.Ö., Brynjólfsson, S., Ásbjörnsdóttir, L. 2022b. Iceland: glacial landforms from the Bølling-Allerød interstadial. In: Palacios, D., Hughes, P., García-Ruiz, J.M., Andrés, N. (Eds.), European Glacial Landscapes, Elsevier, in press.

Benediktsson, Í.Ö., Brynjólfsson, S., Ásbjörnsdóttir, L. 2022c. Glacial landscapes of Iceland from the Younger Dryas. *In*: Palacios, D., Hughes, P., García-Ruiz, J.M., Andrés, N. (Eds.), European Glacial Landscapes, Elsevier, in press.

Briner, J.P. 2007. Supporting evidence from the New York drumlin field that elongate subglacial bedforms indicate fast ice flow. Boreas 36, 143-147. https://doi.org/10.1111/j.1502-3885.2007.tb01188.x

Boulton, G.S. 1987. A theory of drumlin formation by subglacial sediment. In Drumlin Symposium. Balkema, Rotterdam.

Boulton, G. S., Dobbie, K. E., & Zatsepin, S. 2001. Sediment deformation beneath glaciers and its coupling to the subglacial hydraulic system. Quaternary International, *86*(1), 3-28.

Bourgeois, O., Dauteuil, O., Van Vliet-Lanoë, B. 2000. Geothermal control on flow patterns in the last glacial maximum ice sheet of Iceland. Earth Surface Processes and Landforms, 25, 59-76. https://doi.org/10.1002/(SICI)1096-9837(200001)25:1<59::AID-ESP48>3.0.CO;2-T

Bristow, C.S., Jol, H.M. (Eds.). 2003. Ground penetrating radar in sediments. Geological Society of London.

Cassidy, N.J., Russell, A.J., Marren, P.M., et al. 2003. GPR derived architecture of November 1996 jökulhlaup deposits, Skeiðarársandur, Iceland. Geological Society, London, Special Publications, 211(1), 153-166. https://doi.org/10.1144/GSL.SP.2001.211.01.13

Clark, C.D. 1993. Mega-scale glacial lineations and cross-cutting ice-flow landforms. Earth surface processes and landforms, 18(1), 1-29.

Clark, C. 2010. Emergent drumlins and their clones: From till dilatancy to flow instabilities. Journal of Glaciology, 56(200), 1011-1025. doi:10.3189/002214311796406068

Clark, C.D., Spagnolo, M. 2016. Glacially eroded cross-shelf troughs surrounding Iceland from Olex data. In: Dowdeswell, J.A., Canals, M., Jakobsson, M., Todd, B.J., Dowdeswell, E.K., Hogan, K.A. (Eds.). Atlas of Submarine Glacial Landforms: Modern, Quaternary and Ancient. Geological Society, London, Memoirs 46, 165-166. Geological Society of London. https://doi.org/10.1144/M46.86 https://doi.org/10.1016/j.geomorph.2015.02.018

Dowling, T. 2016. The drumlin problem: streamlined subglacial bedforms in southern Sweden. Lund University.

Evans, D.J.A, Twigg, D.R. 2002. The active temperate glacial landsystem: a model based on Breiðamerkurjökull and Fjallsjökull, Iceland. Quaternary science reviews, 21(20-22), 2143-2177. https://doi.org/10.1016/S0277-3791(02)00019-7

Evans, D.J.A., Phillips, E.R., Hiemstra, J.F., et al. 2006. Subglacial till: formation, sedimentary characteristics and classification. Earth-Science Reviews, 78(1-2), 115-176. https://doi.org/10.1016/j.earscirev.2006.04.001

Evans, D.J.A., Benn, D.I. (Eds.). 2004. A practical guide to the study of glacial sediments. 83-87 & 97-107 pp. Arnold, London.

Evans, D.J.A., Roberts, D.H., Cofaigh, C.Ó. 2015. Drumlin sedimentology in a hard-bed, lowland setting, Connemara, western Ireland: implications for subglacial bedform generation in areas of sparse till cover. Journal of Quaternary Science, 30(6), 537-557. https://doi.org/10.1002/jqs.2801

Eyles, N., Putkinen, N., Sookhan, S., et al. 2016. Erosional origin of drumlins and megaridges. Sedimentary Geology 338, 2-23. https://doi.org/10.1016/j.sedgeo.2016.01.006

Finlayson, A. 2013. Digital surface models are not always representative of former glacier beds: palaeoglaciological and geomorphological implications. Geomorphology, 194, 25-33. https://doi.org/10.1016/j.geomorph.2013.03.026

Fowler, A.C. 2000. An instability mechanism for drumlin formation. Geological Society, London, Special Publications, 176(1), 307-319.

Fowler, A.C. 2010. The instability theory of drumlin formation applied to Newtonian viscous ice of finite depth. Proceedings of the Royal Society A: Mathematical, Physical and Engineering Sciences, 466(2121), 2673-2694. https://doi.org/10.1098/rspa.2010.0017

Fowler, A.C. 2018. The philosopher in the kitchen: the role of mathematical modelling in explaining drumlin formation, GFF, 140(2), 93-105. 10.1080/11035897.2018.1444671

Fowler, A.C., Chapwanya, M. 2014. An instability theory for the formation of ribbed moraine, drumlins and mega-scale glacial lineations. Proceedings of the Royal Society A: Mathematical, Physical and Engineering Sciences, 470(2171), 20140185. https://doi.org/10.1098/rspa.2014.0185

Greenwood, S.L., Clark, C.D., Hughes, A.L. 2007. Formalising an inversion methodology for reconstructing ice-sheet retreat patterns from meltwater channels: application to the British

Ice Sheet. Journal of Quaternary Science: Published for the Quaternary Research Association, 22(6), 637-645. https://doi.org/10.1002/jqs.1083

Guðmundsdóttir, E.R., Eiríksson, J., Larsen, G. 2011. Identification and definition of primary and reworked tephra in Late Glacial and Holocene marine shelf sediments off North Iceland. Journal of Quaternary Science, 26(6), 589-602. https://doi.org/10.1002/jqs.1474

Hart, J.K. 1997. The relationship between drumlins and other forms of subglacial glaciotectonic deformation. Quaternary Science Reviews, 16(1), 93-107. https://doi.org/10.1016/S0277-3791(96)00023-6

Hart, J.K. 1999. Identifying fast ice flow from landform assemblages in the geological record: a discussion. Annals of Glaciology, 28, 59-66. doi:10.3189/172756499781821887

Hermanowski, P., Piotrowski, J.A., Szuman, I. 2019. An erosional origin for drumlins of NW Poland. Earth Surface Processes and Landforms, 44(10), 2030-2050. https://doi.org/10.1002/esp.4630

Hindmarsh, R. 1998. Drumlinization and drumlin-forming instabilities: Viscous till mechanisms. Journal of Glaciology, 44(147), 293-314. doi:10.3189/S002214300000263X

Hubbard, A., Sugden, J., Dugmore, A., et al. 2006. A modelling insight into the Icelandic Late Glacial Maximum ice sheet. Quaternary Science Reviews, 25(17-18), 2283-2296. https://doi.org/10.1016/j.quascirev.2006.04.001

Icelandic Institute of Natural History, 2019. Geological map of Iceland. Bedrock. 1st edition. Geology of Iceland. http://jardfraedikort.ni.is (checked 2021-07-05).

Ingólfsson, Ó., Norðdahl, H. 2001. High relative sea-level during the Bølling interstadial in W Iceland: a reflection of ice-sheet collapse and extremely rapid glacial unloading. Arctic, Antarctic and Alpine Research, 33, 231-243. https://doi.org/10.1080/15230430.2001.12003426

Iverson, N.R., McCracken, R.G., Zoet, L., et al. 2017. A theoretical model of drumlin formation based on observations at Múlajökull, Iceland. Journal of Geophysical Research Earth Surface, 122. https://doi.org/10.1002/2017JF004354.

Johnson, M.D., Schomacker, A., Benediktsson, Í.Ö., et al. 2010. Active drumlin field revealed at the margin of Múlajökull, Iceland: a surge-type glacier. Geology, 38, 943-946. https://doi.org/10.1130/G31371.1

Jóhannesson, H., Sæmundsson, K. 2009. Geological map of Iceland. 1:500.000. Bedrock (1st edition). Icelandic Institute of Natural History. Reykjavík.

Jol, H.M., Bristow, C.S. 2003. GPR in sediments: advice on data collection, basic processing and interpretation, a good practice guide. SPECIAL PUBLICATION-GEOLOGICAL SOCIETY OF LONDON, 211, 9-28.

Jónsson, S.A., Benediktsson, Í.Ö., Ingólfsson, Ó., et al. 2016. Submarginal drumlin formation and late Holocene history of Fláajökull, southeast Iceland. Annals of Glaciology, 57 (72), 128-141. doi:10.1017/aog.2016.4

King, E., Woodward, J., Smith, A. 2007. Seismic and radar observations of subglacial bed forms beneath the onset zone of Rutford Ice Stream, Antarctica. Journal of Glaciology, 53(183), 665-672. doi:10.3189/002214307784409216

Kjær, K.H., Krüger, J. 1998. Does clast size influence fabric strength?. Journal of Sedimentary Research, 68(5), 746-749. https://doi.org/10.2110/jsr.68.746

Kjær, K.H., Sultan, L., Krüger, J., et al. 2004. Architecture and sedimentation of outwash fans in front of the Mýrdalsjökull ice cap, Iceland. Sedimentary Geology, 172(1-2), 139-163. https://doi.org/10.1016/j.sedgeo.2004.08.002

Kjær, K. H., Larsen, E., van der Meer, J., et al. 2006. Subglacial decoupling at the sediment/bedrock interface: a new mechanism for rapid flowing ice. Quaternary Science Reviews, *25*(21-22), 2704-2712.

Krüger, J., Kjær, K.H. 1999. A data chart for field description and genetic interpretation of glacial diamicts and associated sediments - with examples from Greenland, Iceland, and Denmark. Boreas, 28(3), 386-402. https://doi.org/10.1111/j.1502-3885.1999.tb00228.x

Lawson, D.E. 1979. A comparison of the pebble orientations in ice and deposits of the Matanuska Glacier, Alaska. The Journal of Geology, 87(6), 629-645.

Livingstone, S.J., Cofaigh, C.Ó., Stokes, C.R., et al. 2012. Antarctic palaeo-ice streams. Earth-Science Reviews, 111(1-2), 90-128. https://doi.org/10.1016/j.earscirev.2011.10.003

Maclachlan, J.C., Eyles, C.H. 2013. Quantitative geomorphological analysis of drumlins in the Peterborough drumlin field, Ontario, Canada. Geografiska Annaler: Series A, Physical Geography, 95(2), 125-144. https://doi.org/10.1111/geoa.12005

McCracken, R.G., Iverson, N.R., Benediktsson, Í.Ö., et al. 2016. Origin of the active drumlin field at Múlajökull, Iceland: new insights from till shear and consolidation patterns. Quaternary Science Reviews, 148, 243-260. https://doi.org/10.1016/j.quascirev.2016.07.008

Menzies, J. 1979. A review of the literature on the formation and location of drumlins. Earth-Science Reviews, 14(4), 315-359.

Menzies, J., Brand, U. 2007. The internal sediment architecture of a drumlin, Port Byron, New York State, USA. Quaternary Science Reviews, 26(3-4), 322-335. https://doi.org/10.1016/j.quascirev.2006.07.003

Menzies, J., Hess, D.P., Rice, J.M., et al. 2016. A case study in the New York Drumlin Field, an investigation using microsedimentology, resulting in the refinement of a theory of drumlin formation. Sedimentary Geology, 338, 84-96.

Möller, P., Dowling, T.P. 2016. Streamlined subglacial bedforms on the Närke plain, south-central Sweden–areal distribution, morphometrics, internal architecture and formation. Quaternary Science Reviews, 146, 182-215. https://doi.org/10.1016/j.quascirev.2016.04.007

Napieralski, J., Nalepa, N. 2010. The application of control charts to determine the effect of grid cell size on landform morphometry. Computers & Geosciences 36, 222-230.

Neal, A. 2004. Ground-penetrating radar and its use in sedimentology: principles, problems and progress. Earth-science reviews, 66(3-4), 261-330. https://doi.org/10.1016/j.earscirev.2004.01.004

Norðdahl, H., Hjort, C. 1993. Lateglacial raised beaches and glacier recession in the Þistilfjörður-Bakkaflói area. Jökull, 43, 32-44.

Norðdahl, H., Pétursson, H.G. 2005. Relative sea-level changes in Iceland. New aspects of the Weichselian deglaciation of Iceland. In: Caseldine C, Russel A, Harðardóttir J, Knudsen Ó (Eds.), Iceland – modern processes and past environments. Elsevier, Amsterdam, pp. 25-78.

Norðdahl, H., Ingólfsson, Ó., Pétursson, H.G., et al. 2008. Late Weichselian and Holocene environmental history of Iceland. Jökull, 58, 343-364.

Norðdahl, H., Ingólfsson, Ó. 2015. Collapse of the Icelandic ice sheet controlled by sea-level rise? Arktos, 1, 1-18. https://doi.org/10.1007/s41063-015-0020-x

Norðdahl, H., Ingólfsson, Ó., Vogler, E.D., et al. 2019. Glacio-isostatic age modelling and Late Weichselian deglaciation of the Lögurinn basin, East Iceland. Boreas, 48(3), 563-580. https://doi.org/10.1111/bor.12366

Patton, H., Hubbard, A., Bradwell, T., et al. 2017. The configuration, sensitivity and rapid retreat of the Late Weichselian Icelandic ice sheet. Earth-Science Reviews, 166, 223-245. https://doi.org/10.1016/j.earscirev.2017.02.001

Piotrowski, J.A., Larsen, N.K., Junge, F.W. 2004. Reflections on soft subglacial beds as a mosaic of deforming and stable spots. Quaternary Science Reviews, 23(9-10), 993-1000. https://doi.org/10.1016/j.quascirev.2004.01.006

Porter, C., Morin, P., Howat, I., et al. 2018, “ArcticDEM”, https://doi.org/10.7910/DVN/OHHUKH, Harvard Dataverse, V1.

Powers, M.C. 1953. A new roundness scale for sedimentary particles. Journal of Sedimentary Research, 23(2), 117-119.

Principato, S.M., Moyer, A.N., Hampsch, A.G., et al. 2016. Using GIS and streamlined landforms to interpret palaeo-ice flow in northern Iceland. Boreas 45, 470-482. https://doi.org/10.1111/bor.12164

Shaw, J. 2002. The meltwater hypothesis for subglacial bedforms. Quaternary International, 90(1), 5-22. https://doi.org/10.1016/S1040-6182(01)00089-1

Smalley, I., Unwin, D. 1968. The Formation and Shape of Drumlins and their Distribution and Orientation in Drumlin Fields. Journal of Glaciology, 7(51), 377-390. doi:10.3189/S0022143000020591

Smith, A.M. 1997. Basal conditions on Rutford ice stream, West Antarctica, from seismic observations. Journal of Geophysical Research: Solid Earth, 102(B1), 543-552.

Smith, A.M., Murray, T., Nicholls, K.W., et al. 2007. Rapid erosion, drumlin formation, and changing hydrology beneath an Antarctic ice stream. Geology, *35*(2),127-130. https://doi.org/10.1130/G23036A.1

Spagnolo, M., Clark C.D. 2009. A geomorphological overview of glacial landforms on the Icelandic continental shelf. Journal of Maps, 2009, 37-52. https://doi.org/10.4113/jom.2009.1049

Spagnolo, M., Clark, C.D., Hughes, A.L., et al. 2010. The planar shape of drumlins. Sedimentary Geology, 232(3-4), 119-129. https://doi.org/10.1016/j.sedgeo.2010.01.008

Spagnolo, M., Clark, C.D., Hughes, A.L. 2012. Drumlin relief. Geomorphology, 153, 179-191. https://doi.org/10.1016/j.geomorph.2012.02.023

Spagnolo, M., King, E.C., Ashmore, D.W., et al. 2014. Looking through drumlins: testing the application of ground-penetrating radar. Journal of Glaciology, 60(224), 1126-1134. doi:10.3189/2014JoG14J110

Stokes, C.R., Clark. C.D. 1999. Geomorphological criteria for identifying Pleistocene ice streams. Annals of Glaciology, 28, 67-74. doi:10.3189/172756499781821625

Stokes, C.R., Clark, C.D. 2001. Palaeo-ice streams. Quaternary Science Reviews 20, 1437-1457. https://doi.org/10.1016/S0277-3791(01)00003-8

Stokes, C.R., Clark, C.D. 2002. Are long subglacial bedforms indicative of fast ice flow? Boreas, 31(3), 239-249.

Stokes, C.R., Clark, C.D., Lian, O.B., et al. 2007. Ice stream sticky spots: a review of their identification and influence beneath contemporary and palaeo-ice streams. Earth-Science Reviews, 81(3-4), 217-249. https://doi.org/10.1016/j.earscirev.2007.01.002

Stokes, C.R., Lian, O.B., Tulaczyk, S., et al. 2008. Superimposition of ribbed moraines on a palaeo-ice-stream bed: implications for ice stream dynamics and shutdown. Earth Surface Processes and Landforms: The Journal of the British Geomorphological Research Group, 33(4), 593-609. https://doi.org/10.1002/esp.1671

Stokes, C.R., Spagnolo, M., Clark, C.D. 2011. The composition and internal structure of drumlins: complexity, commonality, and implications for a unifying theory of their formation. Earth-Science Reviews, 107(3-4), 398-422. https://doi.org/10.1016/j.earscirev.2011.05.001

Stokes, C.R., Fowler, A.C., Clark, C.D., et al. 2013. The instability theory of drumlin formation and its explanation of their varied composition and internal structure. Quaternary Science Reviews, 62, 77-96. https://doi.org/10.1016/j.quascirev.2012.11.011

Stokes, C.R. 2018. Geomorphology under ice streams: Moving from form to process. Earth Surfaces Processes and Landforms, 43, 85-123. https://doi.org/10.1002/esp.4259

Sæmundsson, K. 1977. Geological Map of Iceland, Sheet 7, NE-Iceland. 1:250.000. Icelandic Institute of Natural History and National Land Survey of Iceland, Reykjavik.

Sæmundsson, Th. 1995. Deglaciation and shoreline displacement in Vopnafjörður, northeastern Iceland. LUNDQUA thesis 33,1-106. Department of Quaternary Geology, Lund University.

Waller, R.I., Van Dijk, T.A., Knudsen, O. 2008. Subglacial bedforms and conditions associated with the 1991 surge of Skeiðarárjökull, Iceland. Boreas, 37(2), 179-194. https://doi.org/10.1111/j.1502-3885.2007.00017.x

Watts, H., Booth, A.D., Reinardy, B.T., et al. 2022. An Assessment of Geophysical Survey Techniques for Characterising the Subsurface Around Glacier Margins, and Recommendations for Future Applications. Frontiers in Earth Science, 10. Article 734682. https://doi.org/10.3389/feart.2022.734682

Woodard, J.B., Zoet, L.K., Benediktsson, Í.Ö., et al. 2020. Insights into drumlin development from ground-penetrating radar at Múlajökull, Iceland, a surge-type glacier. Journal of Glaciology, 1–9. https://doi.org/10.1017/jog.2020.50

Table 1. Information of the GPR profiles acquired. The highlighted profiles are considered representative for the GPR dataset and discussed in the manuscript. The additional profiles can be made available upon request.

							Start point		End point		
Drumlin	**Profile ID**	**Antenna (MHz)**	**Antenna separation (m)**	**Step size (m)**	**Length (m)**	**Direction**	**Longitude**	**Latitude**	**Longitude**	**Latitude**	**Geometry**
	5_49	50	4	0.4	800	SW-NE	492528	7276296	493123	7276762	Longitudinal
	5_51	50	4	0.5	215	NW-SE	495882	7276671	493026	7276553	Transversal
	5_53	50	4	0.4	159	NW-SE	492633	7276468	492734	7276369	Transversal
	5_50	50	4	0.4	76	W-E	492632	7276354	492698	7276367	Diagonal
Thury	5_52	50	4	0.4	105	W-NNE	492662	7276360	492759	7276377	Diagonal
	1_69	100	0.6	0.25	691	SW-NE	492608	7276336	493119	7276761	Longitudinal
	1_73	100	0.6	0.25	150	NW-SE	492932	7276657	493018	7276537	Transversal
	1_72	100	0.6	0.25	149	NW-SE	492867	7276616	492967	7276513	Transversal
	1_71	100	0.6	0.25	221	W-E	492611	7276404	492823	7276404	Diagonal
	5_33	50	4	0.02	672	SSW-NNE	484089	7272929	484423	7273416	Longitudinal
	5_34	50	4	0.02	142	SSW-NNE	484258	7273173	484332	7273285	Longitudinal
	5_35	50	4	0.4	631	SSW-NNE	484433	7273286	484700	7273737	Longitudinal
	5_36	50	4	0.4	250	WNW-ESE	484345	7273516	484533	7273380	Transversal
	5_32	50	4	0.02	265	WNW-ESE	484144	7273266	484341	7273118	Transversal
Foss	5_37	50	4	0.25	148	WNW-ESE	484195	7272969	484107	7273045	Transversal
	1_1	100	0.6	0.05	884	SSW-NNE	484100	7272947	484587	7273622	Longitudinal
	1_344	100	0.6	0.05	134	WNW-ESE	484108	7273064	484199	7272972	Transversal
	1_345	100	0.6	0.05	251	WNW-ESE	484138	7273267	484339	7273121	Transversal
	1_346	100	0.6	0.05	246	WNW-ESE	484340	7273512	484529	7273361	Transversal
	1_347	100	0.6	0.05	237	WNW-ESE	484245	7273344	484452	7273241	Transversal

Table 2. Morphometrics of drumlins within the Bustarfell drumlin field

n=77	**Mean**	**Median**	**Max**	**Min**	**Stdew**	**10%**	**90%**
Length (m)	696	689	1438	319	229	409	962
Width (m)	183	176	301	86	49	130	262
ER	3.8	3.8	6.5	1.9	1	2.8	5.1
Orientation (°)	36	37	52	3	9	27	46

Table 3. Radar facies description and interpretation.

Facies/Structures Antenna	Example	Description	Lithology	Sedimentological interpretation
A (Structure) 50 MHz		Planar to wavy, moderately continuous reflections	Bedrock contact	Upper boundary of the bedrock (plateau basalts)
B.1 (Facies) 50 MHz		Wavy, moderately continuous to discontinuous reflections	Diamict and sorted sediments	Subglacial traction till and glaciofluvial material
B.2 (Facies) 100 MHz	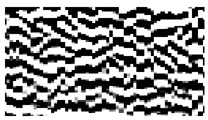	Chaotic, moderately continuous to discontinuous reflections	Diamict and sorted sediments	Subglacial traction till and glaciofluvial material
B.3 (Structure) 50 and 100 MHz		Hyperbolas	Boulder cluster	Boulder or boulder clusters in diamict
C.1 (Structure) 50 MHz		Concave and convex reflections	Gravel and sand layers	Channel infillings
C.2 (Structure) 100 MHz		Concave, subparallel reflections	Gravel and sand layers	Channel infillings
D (Facies) 50 and 100 MHz		Parallel, (vague) reflections that range from being continuous to discontinuous.	Mixed finer grained sediments	Post-glacial sediments

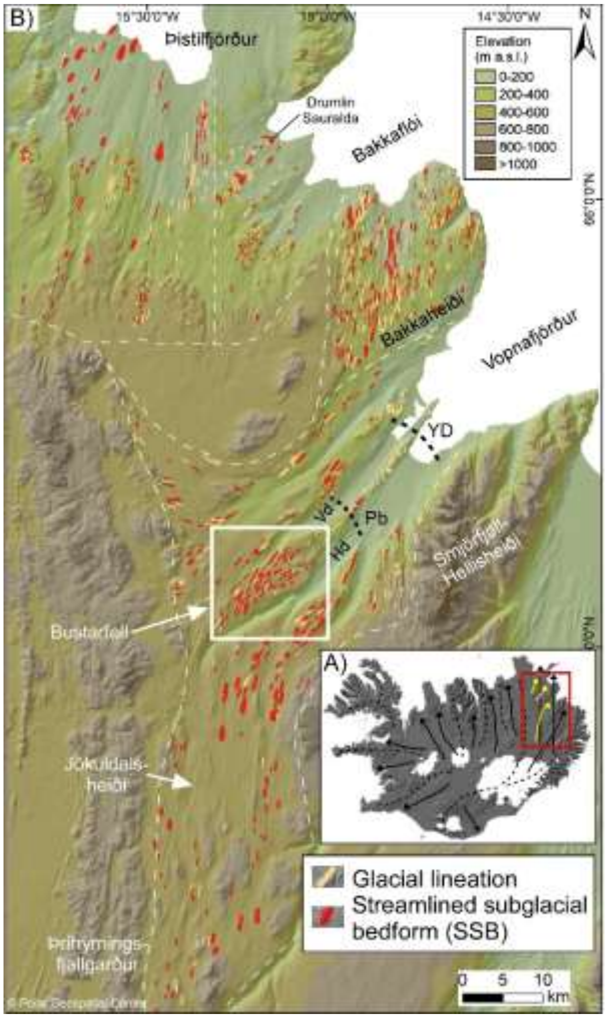

Figure 1. A) Major ice streams of the Iceland Ice Sheet according to Bourgeois et al. (2000), Stokes and Clark (2001) and Principato et al. (2016). In NE-Iceland the black arrows indicate an older generation of ice flow during maximum glaciation while the yellow arrows represent a younger generation during deglaciation (Benediktsson et al., 2022a). Fig. 1B is outlined in red on Fig. 1A. B) Overview map of glacial lineations and streamlined subglacial bedforms (SSBs) in NE-Iceland (modified from Benediktsson et al. 2022a). The white dashed lines indicate boundaries between flow-sets; Þistilfjörður, Bakkaflói, Bakkaheiði, and Vopnafjörður-Jökuldalsheiði with Vesturárdalur (Vd) and Hofsárdalur (Hd) marked. The present study area, the Bustarfell drumlin field, is located within the white box. Ice-marginal positions during the Younger Dryas (YD) and

the Preboreal (Pb) are indicated within the Vopnafjörður valley-fjord based on Sæmundsson (1995). Map base layer: Hillshade of the ArcticDEM (PGC, 2018).

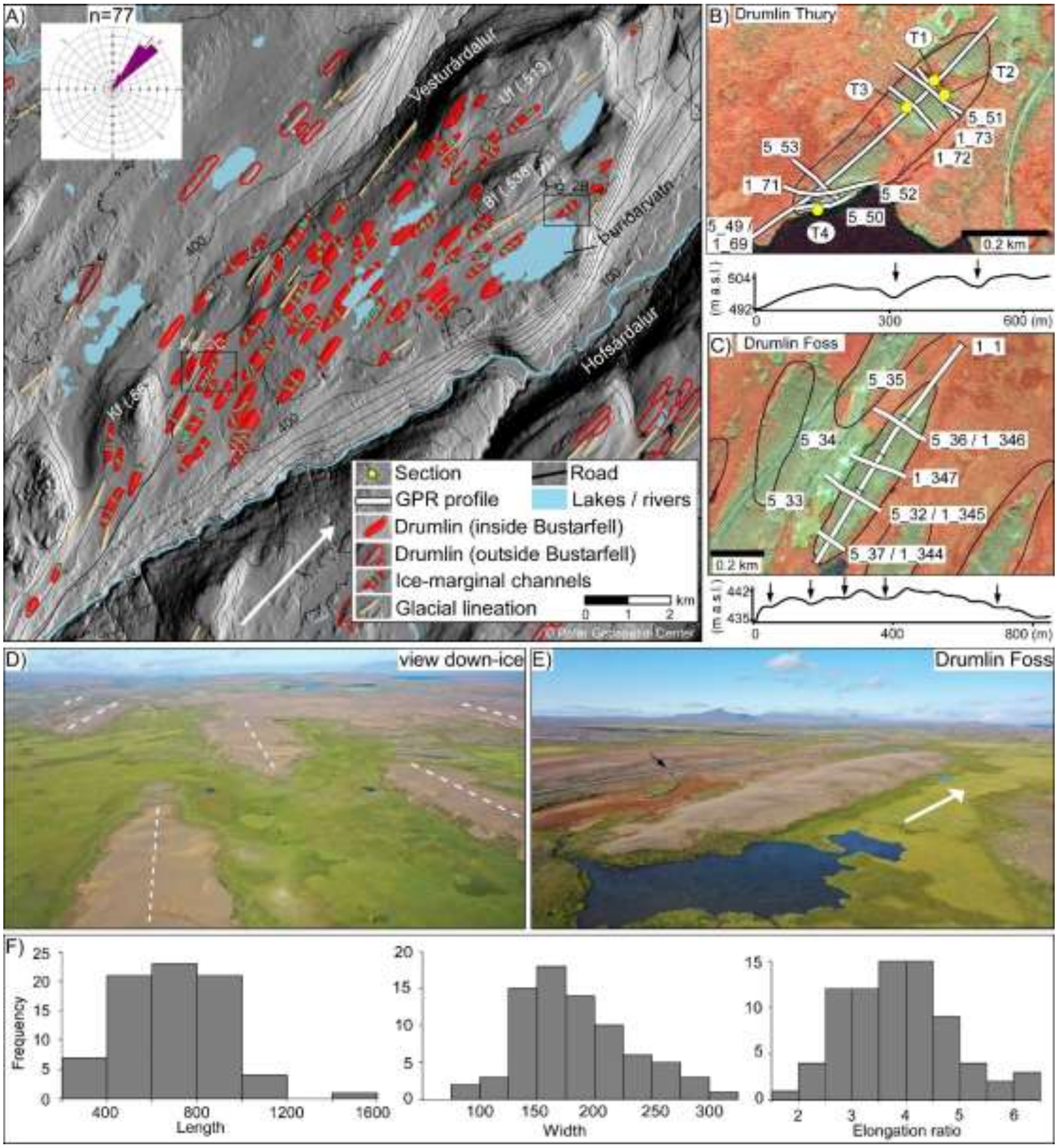

Figure 2. A) The Bustarfell drumlin field within the Vopnafjörður-Jökuldalsheiði flow-set. The rose diagram shows the orientation of the 77 drumlins that have been mapped. Place names referred to in the text are marked and their altitude a.s.l. indicated (Kf-Kálfafell, Bf-Bustarfell, Uf-Urðarfell). The hillshade is from the ArcticDEM with solar angle from the north at 30° and 3 times exaggeration. Contour intervals are 50 m. The legend applies to Fig. A-C..B) Drumlin Thury. C)

Drumlin Foss. Cross profiles are shown below them with arrows pointing at ice-marginal channels. The white lines on B) and C) indicate the locations of the GPR profiles and the number in front of them represent the respective frequency (5:50 MHz, 1:100 MHz). Background data are infrared satellite images from National Land Survey of Iceland. D) Drone image of several drumlins within the Bustarfell drumlin field. The dashed lines indicate the long axes of the most obvious drumlins. E) Drone image of drumlin Foss with a car for scale (black arrow). Note how well-defined the drumlins are within the peat bogs and high ground-water table in the inter-drumlin areas. The white arrows indicate the general ice-flow direction. F) Size-frequency (length, width, and elongation ratio) distribution of the morphometrics of the Bustarfell drumlins.

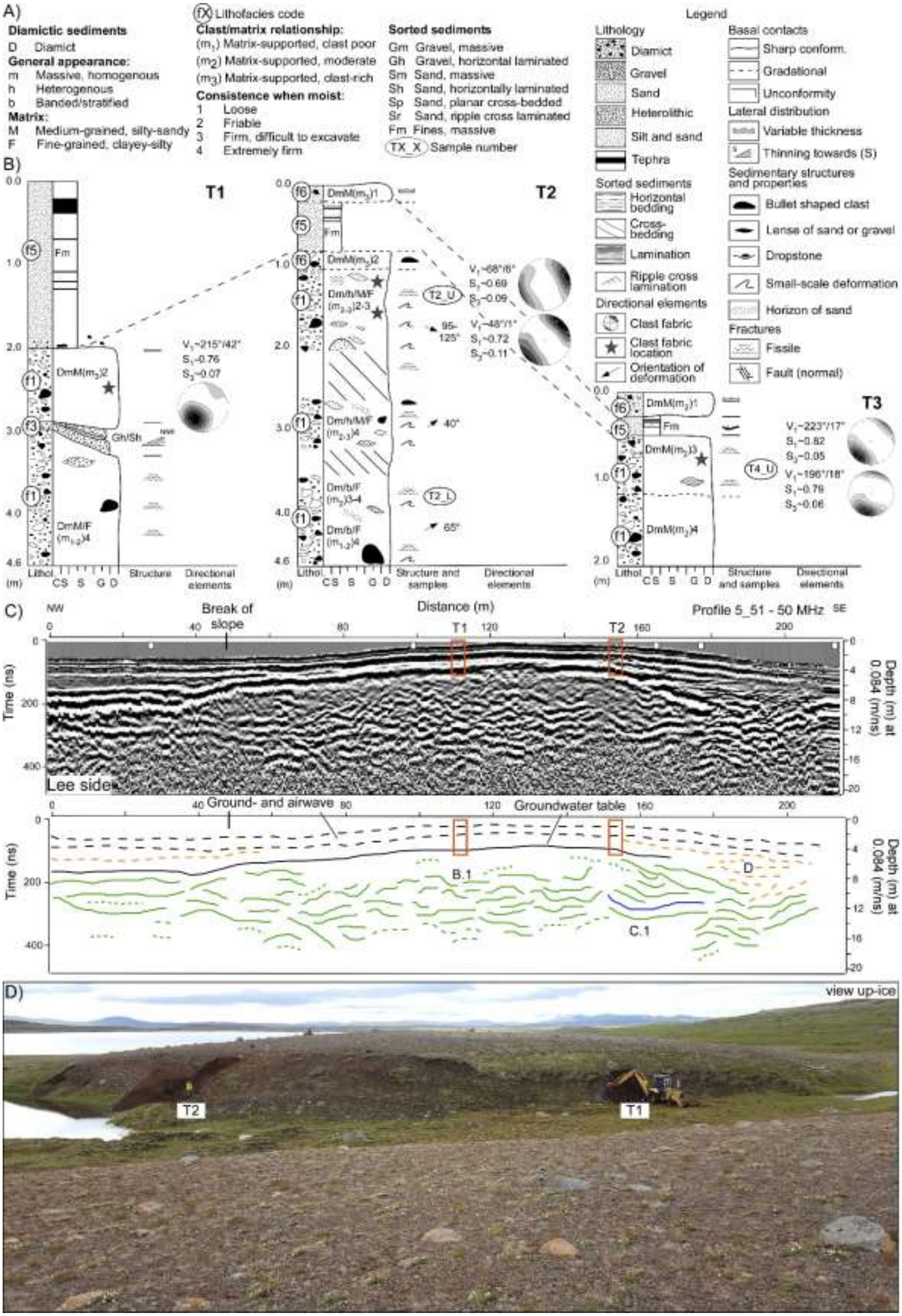

A)
Diamictic sediments
D Diamict
General appearance:
m Massive, homogenous
h Heterogenous
b Banded/stratified
Matrix:
M Medium-grained, silty-sandy
F Fine-grained, clayey-silty
fX Lithofacies code
Clast/matrix relationship:
(m1) Matrix-supported, clast poor
(m2) Matrix-supported, moderate
(m3) Matrix-supported, clast-rich
Consistence when moist:
1 Loose
2 Friable
3 Firm, difficult to excavate
4 Extremely firm
Sorted sediments
Gm Gravel, massive
Gh Gravel, horizontal laminated
Sm Sand, massive
Sh Sand, horizontally laminated
Sp Sand, planar cross-bedded
Sr Sand, ripple cross laminated
Fm Fines, massive
TX_X Sample number
Legend
Lithology
Diamict
Gravel
Sand
Heterolithic
Silt and sand
Tephra
Sorted sediments
Horizontal bedding
Cross-bedding
Lamination
Ripple cross lamination
Directional elements
Clast fabric
Clast fabric location
Orientation of deformation
Basal contacts
Sharp conform.
Gradational
Unconformity
Lateral distribution
Variable thickness
Thinning towards (S)
Sedimentary structures and properties
Bullet shaped clast
Lense of sand or gravel
Dropstone
Small-scale deformation
Horizon of sand
Fractures
Fissile
Fault (normal)
B)
T1
T2
T3
DmM(m3)2
Gh/Sh
DmM/F (m1-2)4
V1~215°/42°
S1~0.76
S3~0.07
DmM(m2)1
DmM(m3)2
Dm/h/M/F (m2-3)2-3
Dm/h/M/F (m2-3)4
Dm/b/F (m2)3-4
Dm/b/F (m1-2)4
T2_U
T2_L
V1~68°/8°
S1~0.69
S3~0.09
V1~48°/1°
S1~0.72
S3~0.11
95-125°
40°
65°
DmM(m2)1
DmM(m2)3
DmM(m2)4
T4_U
V1~223°/17°
S1~0.82
S3~0.05
V1~196°/18°
S1~0.79
S3~0.06
Lithol.
Structure
Directional elements
Structure and samples
C)
NW
Break of slope
Distance (m)
Profile 5_51 - 50 MHz SE
Time (ns)
Depth (m) at 0.084 (m/ns)
Lee side
Ground- and airwave
Groundwater table
B.1
C.1
D
D)
view up-ice
T2
T1

Figure 3. A) Legend with symbols and lithofacies codes used here and for other logs in the paper, following Krüger and Kjær (1999). B) Stratigraphical logs from sections T1, 2 and 3. The dashed lines show the correlation between the different units as made in the field. C) The processed and interpreted GPR profile 5_51 (50 MHz). The location of sections T1 and T2 are marked. The profiles are exaggerated x2 vertically. D) View up-ice of drumlin Thury during the opening of the sections T1-2 with the excavator.

954

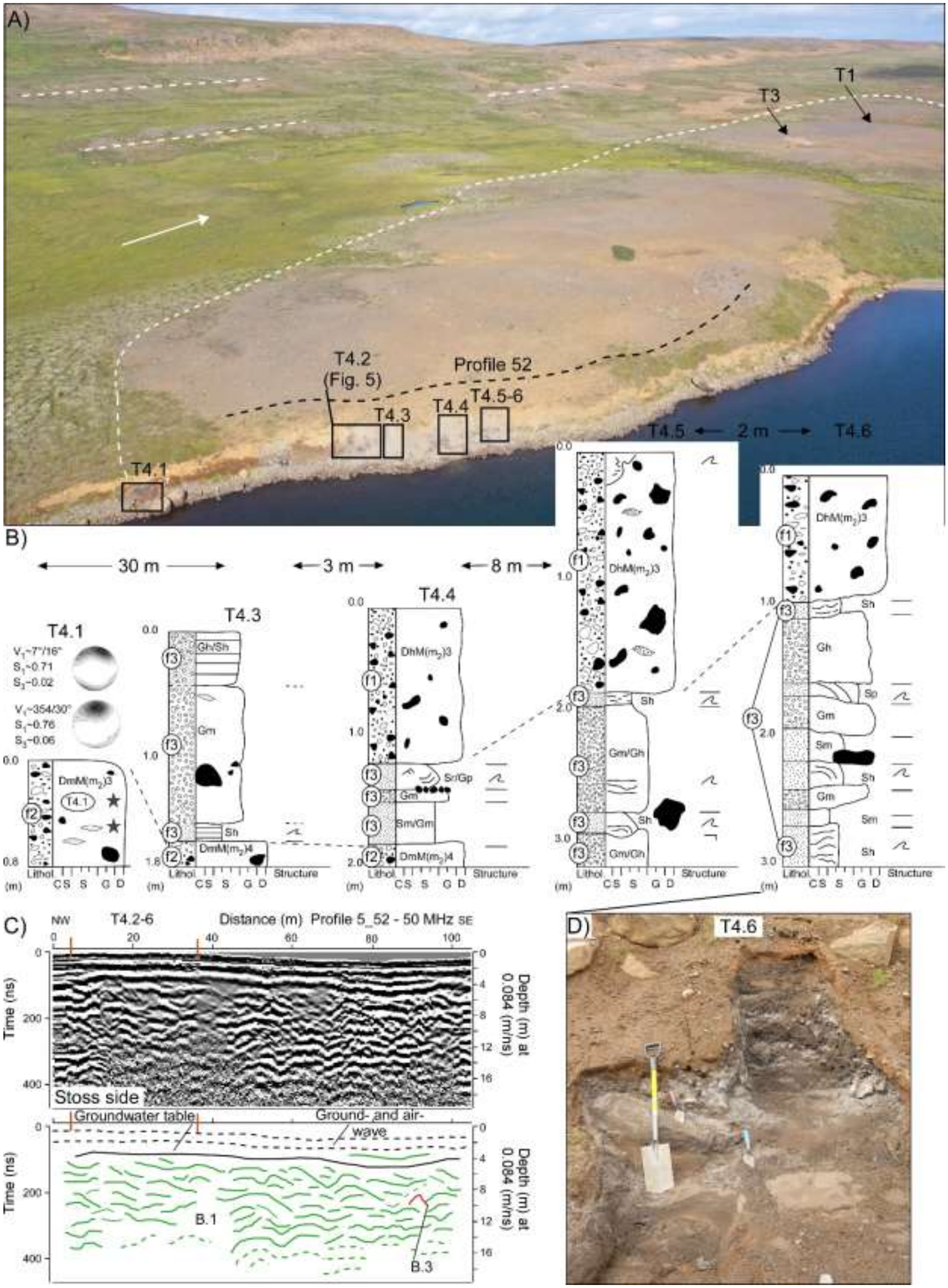

A)
T1
T3
T4.2
(Fig. 5)
Profile 52
T4.3
T4.4
T4.5-6
T4.1
T4.5 ← 2 m → T4.6
B)
← 30 m →
← 3 m →
← 8 m →
T4.1
T4.3
T4.4
DhM(m2)3
DmM(m2)3
DmM(m2)4
Gh/Sh
Gm
Sh
Sr/Gp
Sm/Gm
Gm/Gh
Gh
Sp
Sm
Lithol
Structure
C)
NW
T4.2-6
Distance (m)
Profile 5_52 - 50 MHz
SE
Time (ns)
Depth (m) at 0.084 (m/ns)
Stoss side
Groundwater table
Ground- and air-wave
B.1
B.3
D)
T4.6

Figure 4. A) Drone image of drumlin Thury with view to the north. The different parts of section T4 that have been logged are marked (T4.1-6) together with GPR profile 52. Sections T1 and 2 that are located further down-ice are marked as well. The drumlin and glacial lineations are indicated with white dashed lines to enhance their appearance. The white arrow indicates the general ice-flow direction. B) Stratigraphical logs from section T4. The key to the logs is in Fig. 3A. The dashed lines show the correlation between the different units. C) The processed and interpreted GPR profile 5_52 (50 MHz). The location of sections T4.2-6 are marked. The profile is exaggerated x2 vertically. D) Section T4.6. Note the deformation of the sorted sediments in the lower part.

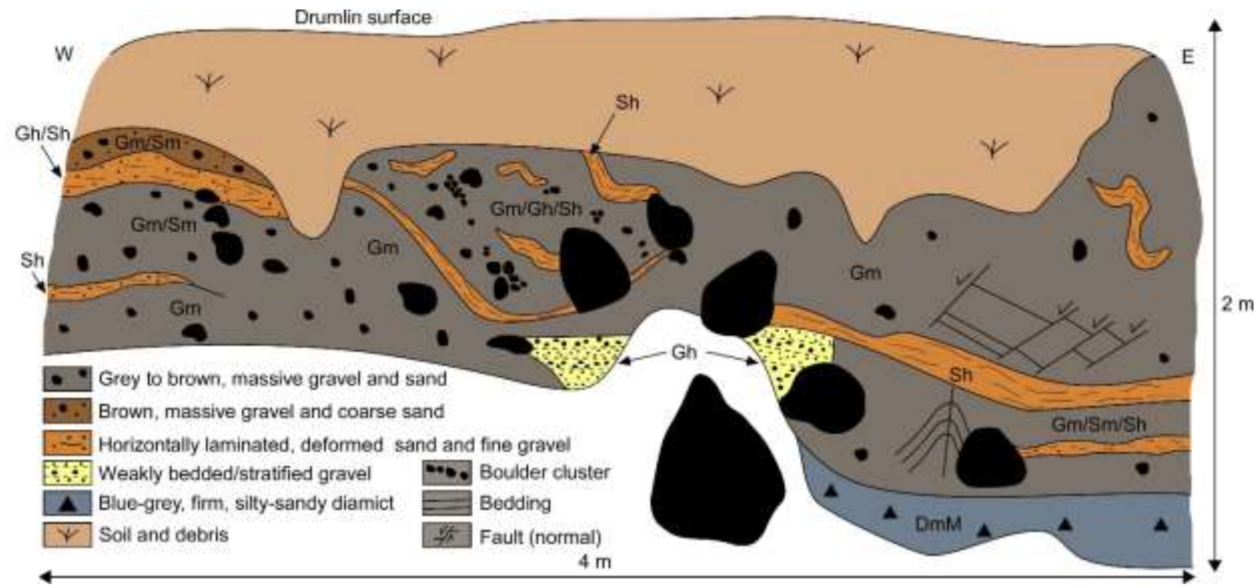

Figure 5. Section T4.2 in drumlin Thury.


A)
Fm
DmM
Gravel lens
Sand lens
Dm/h/M/F
B)
69 cm
31 cm
C)
Fm
DmM
Gh/Sh
DmM/F
D)
DhM
Sh
Gm/Gh
Sh
Gm/Gh
E)
Gm/Sm/Sh
F)
DmM

Figure 6. A) The top of section T2. Note the deformed sand and gravel lenses and the cryoturbated soil (DmM) between the till (Dm/h/M/F) and the soil (Fm). The ruler is 2 m long. B) A close-up of the fissile structure in subglacial traction till in section T3. C) Section T1 with groundwater at the base (4.6 m depth). Note the stratified gravel and sand layer (Gh/Sh) that intersects the till layers. Note also the tephra layers (black arrows) in the soil (Fm). The ruler is 2 m long. D) Section T4.5 is composed of deformed, massive and stratified sand and gravel layers with heterogenous till with sand and silt lenses (black arrows) on top. E) A close-up of a tight, upright fold in sand and gravel in section T4.2. F) Section T4.1 is composed of massive, dark-grey till.

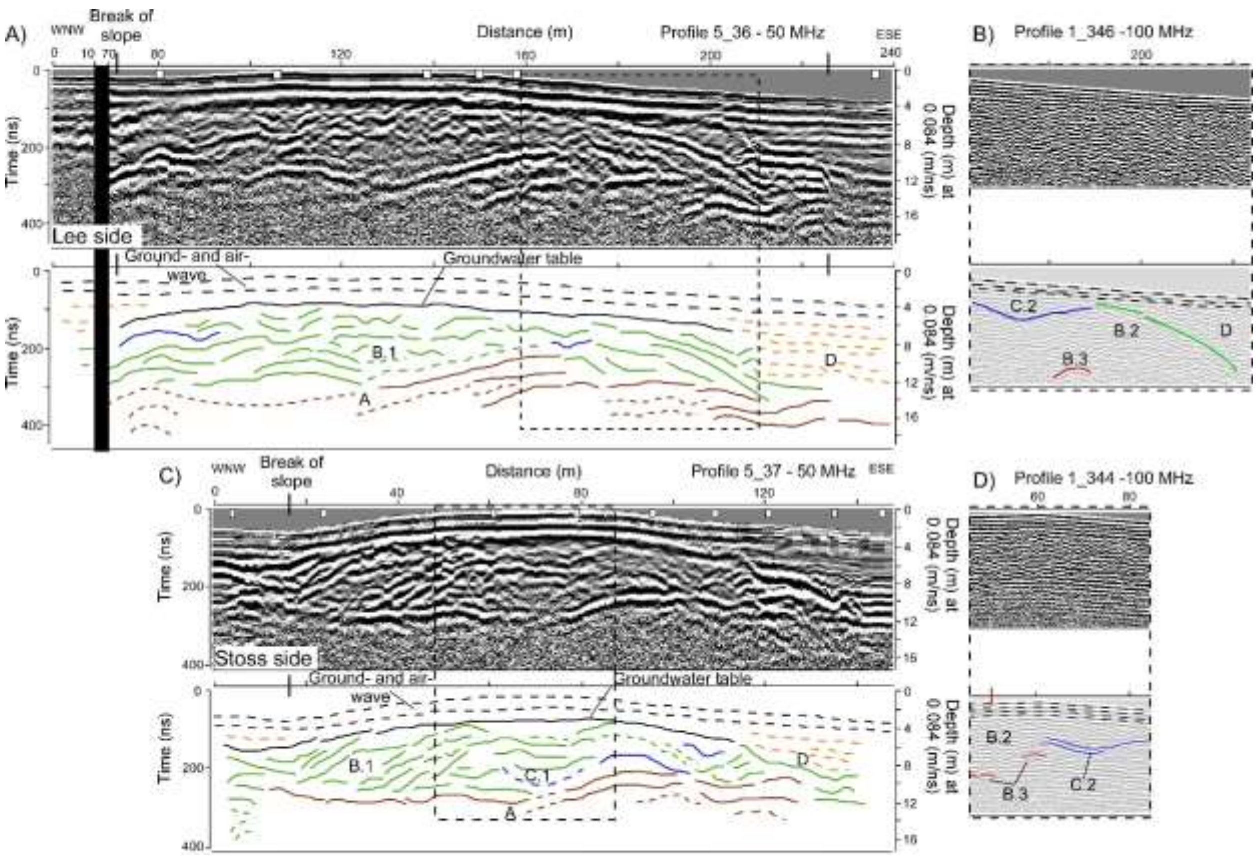

Figure 7. GPR profiles from drumlin Foss (see location on Fig. 2C). A) Profile 5_36, 50 MHz, from the lee side. The black line represents a 60 cm gap that was cut out from the profile. B) A close up of profile 1_346, 100 MHz. C) Profile 5_37, 50 MHz, from the stoss side. The dashed boxes indicate the location of the 100 MHz profiles compared to the 50 MHz. D) A close up of profile 1_344, 100 MHz. Note the correlation of structures between the profiles. Due to the chaotic reflections in radar facies B.2 on the 100 MHz profiles, individual reflections are not drawn but the transparent profile is displayed instead.

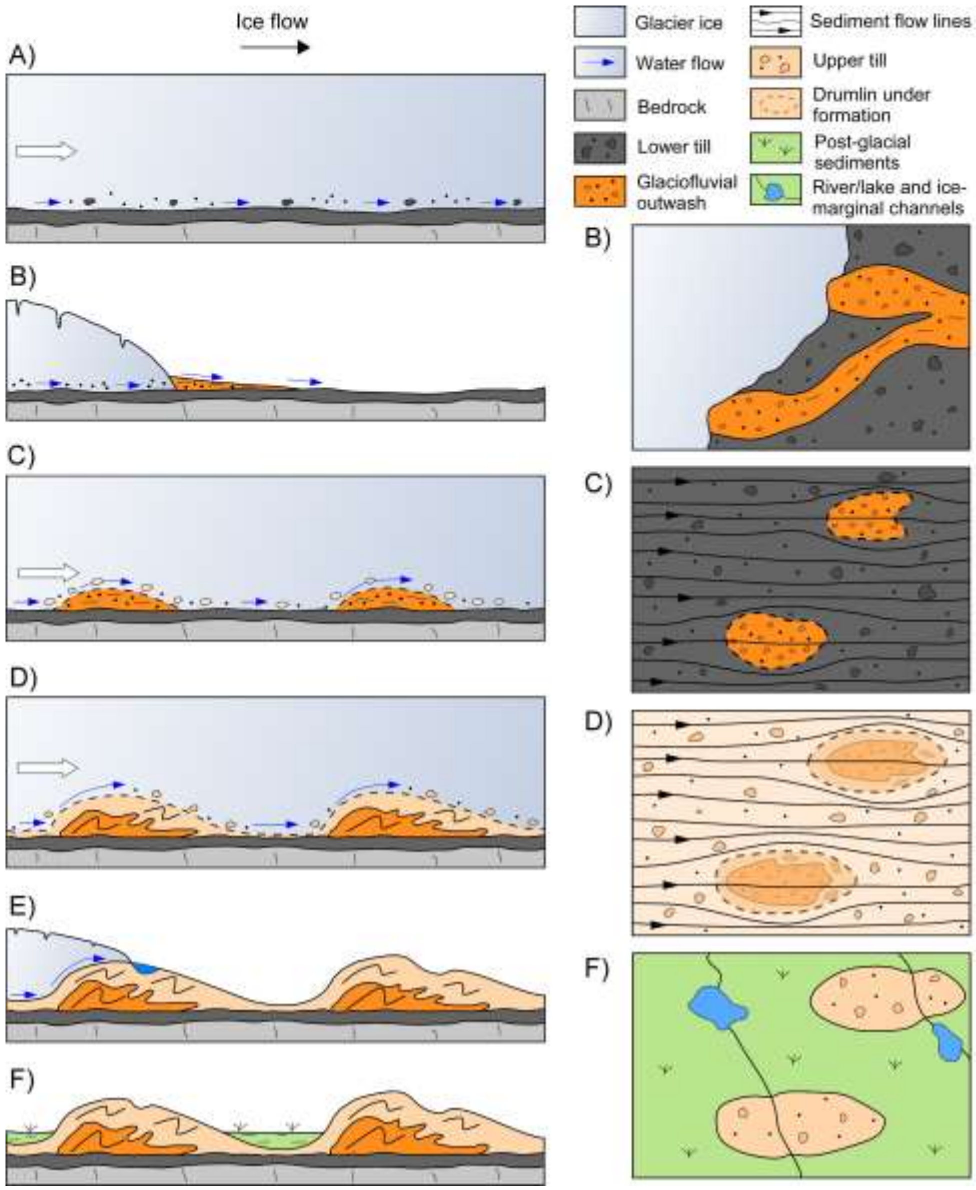

Figure 8. A conceptual model of the formation of the investigated drumlins. A) Maximum glaciation. Deposition of subglacial traction till. B) Deglaciation. Ice-marginal outwash fans are deposited. C) Glacier readvance. The coarser grained glaciofluvial material acts as sticky spots and initiates the drumlin formation. D) Drumlin formation. Deformation of the glaciofluvial core and subglacial traction till is draped around it followed by drumlinisation of the landscape. E) Deglaciation. The ice retreat is stepwise and ice-marginal channels are formed during the retreat.

F) Post-glacial sediments are deposited with time in the inter-drumlin areas. The scale is non proportional.